# Extraction of Bridge Modal Parameters Using Passing Vehicle Response

Chengjun Tan, S.M.ASCE<sup>1</sup>; Nasim Uddin, P.E., F.ASCE<sup>2</sup>; Eugene J. OBrien<sup>3</sup>; Patrick J. McGetrick<sup>4</sup>; and Chul-Woo Kim<sup>5</sup>

**Abstract:** Bridge modal parameters play an important role in bridge engineering; they can serve as useful indices for many applications, such as numerical mode calibration and updating, and bridge structural health monitoring (SHM). Recently, the indirect monitoring of bridges has been increasingly investigated and developed because it avoids the need for instrumentation on all bridges of a network. The natural frequencies of bridges have been extracted from the dynamic response of a vehicle numerically and in laboratory experiments. This study proposes an algorithm to extract the bridge mode shapes and damping ratio using similar indirect measurements enhanced by the Hilbert transform (HT). The theoretical closed-form equations are derived for a vehicle—bridge interaction (VBI) model in which the vehicle is represented as a moving sprung mass passing over a simply supported beam at a constant low speed. Then, a numerical simulation with a quarter-car model is adopted to verify the proposed algorithm, including case studies on the influence of the vehicle speed and road roughness. In addition, a laboratory test is conducted to further investigate the feasibility of the proposed algorithm. **DOI: 10.1061/(ASCE)BE.1943-5592.0001477.** © 2019 American Society of Civil Engineers.

**Author keywords:** Structural health monitoring (SHM); Bridge; Modal parameters; Drive-by; Hilbert transform (HT); Vehicle-bridge interaction (VBI).

#### Introduction

Bridge structures are an intrinsic part of any transportation network. Assessing the condition of these structures is essential to ensure the required level of safety and effective operation of transport facilities. To maintain the bridge structural integrity, it is necessary to estimate the extent and location of structural damage through periodic monitoring. Over the past two decades, as an alternative to manual inspection, there is increasing interest in electronic monitoring of bridges. This is referred to as structural health monitoring (SHM) and is often obtained from modal parameters of the bridge from dynamic vibration (Carden and Fanning 2004; Chang et al. 2003; Chrysostomou and Stassis 2008; Doebling et al. 1998; Magalhães et al. 2012). Generally, to identify the bridge modal parameters, a large number of sensors need to be installed directly on the bridge deck to record dynamic responses through vibration

<sup>5</sup>Professor, Dept. of Civil and Earth Resources Engineering, Kyoto Univ., Kyoto 606-8501, Japan. ORCID: https://orcid.org/0000-0002-2727-6037. Email: kim.chulwoo.5u@kyoto-u.ac.jp

Note. This manuscript was submitted on January 7, 2019; approved on May 3, 2019; published online on July 3, 2019. Discussion period open until December 3, 2019; separate discussions must be submitted for individual papers. This paper is part of the *Journal of Bridge Engineering*, © ASCE, ISSN 1084-0702.

experiments. Many related research projects, both numerical and experimental, have been performed (Deng and Cai 2009; Grande and Imbimbo 2016; Magalhães et al. 2012).

Recently, the idea of indirect measurement for bridge monitoring, which was first proposed by Yang et al. (2004a), has gained popularity as a field of research. This idea refers to use of the response measured indirectly in a passing vehicle to extract dynamic properties of bridges (Lin and Yang 2005; Yang and Lin 2005). Via vehicle/bridge dynamic interaction, the vehicle suspension system is excited by the bridge displacement and by the surface roughness (Malekjafarian and Obrien 2017; Wang et al. 2016). Therefore, it is possible to identify the bridge modal parameters from the indirect measurement, if there is enough measurement time and a sufficiently smooth road surface profile. Compared with the traditional approaches, in which a limited number of sensors are mounted on the bridge, the indirect approach offers much more spatial information, as well as higher resolution in mode shapes, because the instrumented vehicle can receive the vibration characteristics of each point as it passes over the entire bridge (Deng and Cai 2010; Yang et al. 2014). In principal, only one sensor needs to be deployed on the vehicle.

Through this concept of indirect measurement, the natural frequencies of bridges have been extracted from the dynamic responses of vehicles, both numerically and in practice (Deng et al. 2019; McGetrick et al. 2009; Tan et al. 2017, 2018; Yang and Chang 2009; Yang and Lin 2005). A small number of studies estimated the bridge damping ratio using an instrumented vehicle (González et al. 2012; Keenahan et al. 2014; McGetrick et al. 2009). McGetrick et al. (2009) showed that in the spectra of vehicle accelerations, the intensity of power spectral density (PSD) at both bridge and vehicle frequency peaks decreases with increased bridge damping. As a result, the changes in the magnitude of PSD can be used as an indicator of bridge damage (Keenahan et al. 2014). In a theoretical study, González et al. (2012) adopted a half-car vehiclebridge interaction (VBI) model with a road profile to assess bridge damping by minimizing the sum of squared errors, hence, estimating damping.

<sup>&</sup>lt;sup>1</sup>Graduate Research Assistant and Ph.D. Candidate, Univ. of Alabama at Birmingham, Birmingham, AL 35205 (corresponding author). Email: tan1990@uab.edu

<sup>&</sup>lt;sup>2</sup>Chief Editor, Dept. of Civil, Construction, and Environmental Engineering, Univ. of Alabama at Birmingham, Birmingham, AL 35205. Email: nuddin@uab.edu

<sup>&</sup>lt;sup>3</sup>Professor, School of Architecture, Landscape, and Civil Engineering, Univ. College Dublin, Dublin 4, Ireland. ORCID: https://orcid.org/0000-0002-6867-1009. Email: eugene.obrien@ucd.ie

<sup>&</sup>lt;sup>4</sup>Professor, School of Planning, Architecture and Civil Engineering, Queen's Univ. Belfast, Belfast BT9 5AG, UK. ORCID: https://orcid.org/0000-0001-5373-2334. Email: p.mcgetrick@qub.ac.uk

In an alternative strategy, a number of researchers have studied the feasibility of constructing the bridge mode shapes using indirect measurements (Kong et al. 2016, 2017; Malekjafarian and Obrien 2014, 2017; Marulanda et al. 2017; Obrien and Malekjafarian 2016; Oshima et al. 2014; Yang et al. 2014; Zhang et al. 2012). Zhang et al. (2012) first attempted an indirect approach to the extraction of mode shape-related characteristics of a bridge to verify its feasibility numerically and experimentally. They proposed the installation of a controllable shaker on a vehicle and the recording of the applied forces. Oshima et al. (2014) proposed a multiaxle truck-trailer convoy system for bridge damage detection and estimated the mode shape using an indirect approach. The vehicles perform two functions, both exciting the bridge and measuring the response to that excitation at three or more moving points simultaneously. For N trailers, N segments of bridge response are recorded at the same time at different locations on the bridge. By applying singular value decomposition to these signals, a mode shape vector containing N components, corresponding to the defined areas, are identified for each mode. This approach finds the mode shapes with low resolution.

Malekjafarian and Obrien (2017) proposed a novel algorithm that uses short time frequency domain decomposition to estimate bridge mode shapes from the dynamic response of the vehicle, which is an improvement on the concept proposed by Malekjafarian and Obrien (2014). However, it has only been verified in numerical studies so far. Kong et al. (2016) proposed and numerically verified a method that used a specialized vehicle consisting of a tractor and two following trailers to extract the bridge modal properties, which can overcome the effect of road roughness and driving-related frequencies from the vehicle response. Marulanda et al. (2017) developed a mode shape identification approach using mobile sensors under harmonic excitation.

Yang et al. (2014) theoretically developed the possibility of constructing the bridge mode shapes directly from a transform of the measured response on a passing vehicle; they used the Hilbert transform (HT). This algorithm is considered as a single-input–single-output system in which the bridge is only excited by one moving point under the wheel and the response is measured at the same point. It neglects bridge damping, which is found to have a nonnegligible impact on the extracted mode shapes.

This study proposes an HT-based algorithm to extract the damping ratios and mode shapes of bridges from indirect measurements considering the bridge damping. First, the theoretical closed-form solution is derived based on a simple VBI model in which the vehicle is represented by a moving sprung mass and is passing over a simply supported beam at a constant low speed. Then, through numerical simulation, the feasibility of the new approach is demonstrated and the factors that affect the accuracy of the proposed algorithm are investigated. Finally, a laboratory experiment is performed to further demonstrate the feasibility of the proposed algorithm.

## HT

The HT of a function, s(t), is defined by

$$\widehat{s}(t) = H(s(t)) = \frac{1}{\pi} P \cdot V \cdot \int_{-\infty}^{+\infty} \frac{s(\tau)}{t - \tau} d\tau \tag{1}$$

where  $P \cdot V \cdot$  = Cauchy principal value. In practice, HT is defined as the convolution of s(t) with a unit impulse function of  $P \cdot V \cdot 1/\pi t$ . The HT has a particularly simple representation in the frequency domain: it imparts a phase shift of 90° to every Fourier component of a function, i.e.,  $H(\cos(\omega t)) = \cos(\omega t - \pi/2)$ , where  $\omega > 0$ . Using the signal of s(t) and  $\widehat{s}(t)$ , one can obtain an analytical signal,

z(t), which is represented by the sum of real and imaginary parts, as follows:

$$z(t) = s(t) + i\widehat{s}(t) = A(t)e^{i\theta(t)}$$
(2)

where

$$A(t) = \sqrt{s^2(t) + \hat{s}^2(t)}; \theta(t) = \tan^{-1}\left(\frac{\hat{s}(t)}{s(t)}\right)$$
(3)

The time-dependent functions, A(t) and  $\theta(t)$ , represent the instantaneous amplitude and instantaneous phase of the analytical signal, respectively. It is well known that the instantaneous amplitude function, A(t), can be regarded as the envelope function of s(t) (Huang 2014). The HT has the basic property of linearity, i.e., if  $a_1$  and  $a_2$  are arbitrary (complex) scalars, and  $g_1(t)$  and  $g_2(t)$  are signals, then

$$H(a_1 g_1(t) + a_2 g_2(t)) = a_1 \widehat{g}_1(t) + a_2 \widehat{g}_2(t)$$
(4)

Further, the HT behaves well with respect to convolution, since

$$H(g_1(t) \times g_2(t)) = \hat{g}_1(t) \times g_2(t) = g_1(t) \times \hat{g}_2(t)$$
 (5)

# **Theoretical Formula and Algorithm**

# Analytical Theory

To highlight the dynamic characteristics of the coupled VBI, a simply supported beam traversed by a sprung mass vehicle is considered (Fig. 1) (Brady et al. 2006; Frýba 2014). The following assumptions are adopted without losing the generality of the problem: (1) the beam is of the Bernoulli-Euler type with constant cross section; (2) only a single moving vehicle is considered passing on the beam at any one time; (3) the vehicle mass is assumed to be small compared with that of the bridge, and the inertial effect of the vehicle is neglected; (4) the vehicle passes over the beam at a constant speed; (5) the damping of the beam is of the Rayleigh type; (6) road roughness is ignored in the derivation; and (7) before the arrival of the vehicle, the bridge is at rest.

As presented in Fig. 1, the vehicle is simply modeled as a lumped mass,  $m_{\nu}$ , supported by a spring of stiffness,  $k_{\nu}$ , and it passes over a simply supported beam of length L. The modeled beam is assumed to be of constant mass density  $\overline{m}$  per unit length, have constant bending rigidity EI, external damping coefficient  $c_{b,e}$ , and internal damping coefficient  $c_{b,i}$ . The external damping represents boundary influences, such as damping caused by friction in some types of bearing; the internal damping system characterizes the viscoelastic properties of the material. Based on these assumptions, the equations of motion for the bridge and vehicle are

$$\overline{m}\ddot{u} + c_{b,e}\dot{u} + c_{b,i}I \ \dot{u}^{m} + EIu^{m} = f_c(t)\delta(x - vt)$$
 (6)

$$m_{\nu}\ddot{q}_{\nu} + k_{\nu}(q_{\nu} - u|_{\nu = \nu t}) = 0$$
 (7)

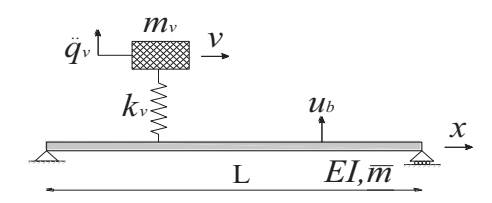


Fig. 1. Theoretical model of vehicle and bridge.

where u(x,t) = vertical displacement of the modeled beam;  $q_v(t)$  = vertical displacement of the vehicle, measured from its static equilibrium position; and a dot and a prime represent the derivative with respect to time t and with respect to longitudinal coordinate x, respectively.

With the assumption that the bridge mass is much greater than the vehicle mass  $(m_v/\overline{m}L \ll 1)$ , the total displacement response of the bridge to the moving vehicle can be expressed as (Yang et al. 2004b)

$$u(x,t) = \frac{\Delta_{st,n}}{\sqrt{\left(1 - S_n^2\right)^2 + 4S_n^2 \varepsilon_{b,n}^2}} \times \left[ \sin\left(\frac{n\pi vt}{L} - \alpha\right) \sin\frac{n\pi vt}{L} \right]$$

$$-\frac{S_n}{\sqrt{1-\varepsilon_{b,n}^2}}e^{-\varepsilon_{b,n}\omega_{b,n}t}\sin(\omega_{d,n}t-\beta)\sin\frac{n\pi\nu t}{L}$$
(8)

where  $\omega_{b,n}$  = natural frequency of the bridge for the nth mode;  $\varepsilon_{b,n}$  = corresponding damping ratio;  $\omega_{\nu}$  = vibration frequency of the vehicle;  $\alpha$  and  $\beta$  = phase angles;  $\Delta_{st,n}$  = static deflection induced by the vehicle for the nth mode;  $S_n$  = nondimensional speed parameter; and  $\omega_{d,n}$  = damped frequency of vibration of the beam and

$$\omega_{b,n} = \left(\frac{n\pi}{L}\right)^2 \sqrt{\frac{EI}{m}} \tag{9}$$

$$\varepsilon_{b,n} = 2\overline{m}\,\omega_{b,n} \tag{10}$$

$$\omega_{\nu} = \sqrt{\frac{k_{\nu}}{m_{\nu}}} \tag{11}$$

$$\alpha = \tan^{-1} \left( \frac{2S_n \varepsilon_{b,n}}{1 - S_n^2} \right) \tag{12}$$

$$\beta = \tan^{-1} \left( \frac{2\varepsilon_{b,n} \sqrt{1 - \varepsilon_{b,n}^2}}{1 - S_n^2 - 2\varepsilon_{b,n}^2} \right)$$
 (13)

$$S_n = \frac{n\pi v}{L\omega_{h,n}} \tag{14}$$

$$\Delta_{st,n} = \frac{-2\omega_{\nu}gL^3}{n^4\pi^4EI} \tag{15}$$

$$\omega_{d,n} = \sqrt{1 - \varepsilon_{b,n}^2} \omega_{b,n} \tag{16}$$

Substituting for these terms in the total displacement of the bridge, u(x,t) in Eq. (8), one can obtain the vehicle displacement by Duhamel's integral (Hu and Tang 2005). Differentiating it twice gives the vehicle acceleration response as

$$\ddot{q}_{v}(t) = \sum_{n} \frac{\Delta_{st,n}}{2\sqrt{\left(1 - S_{n}^{2}\right)^{2} + 4S_{n}^{2}\varepsilon_{b,n}^{2}}}$$

$$\times \left\{ \overline{A}_{1,n}\cos\left(\frac{2n\pi\nu t}{L} - \alpha\right) + \overline{A}_{2,n}\cos(\omega_{v}t + \alpha) + \overline{A}_{3,n}\cos(\omega_{v}t - \alpha) + e^{-\varepsilon_{b,n}\omega_{b,n}t} \left[ \overline{A}_{4,n}\cos(\omega_{v}t + \beta) + \overline{A}_{5,n}\sin(\omega_{v}t + \beta) + \overline{A}_{6,n}\cos\left(\omega_{b,n}t + \frac{n\pi\nu t}{L} - \beta\right) + \overline{A}_{7,n}\cos\left(\omega_{b,n}t - \frac{n\pi\nu t}{L} - \beta\right) + \overline{A}_{8,n}\sin(\omega_{b,n}t + n\pi\nu t/L - \beta) + \overline{A}_{9,n}\sin(\omega_{b,n}t - n\pi\nu t/L - \beta) \right] \right\}$$

$$(17)$$

where the coefficients of  $\overline{A}_{6,n}$ ,  $\overline{A}_{7,n}$ ,  $\overline{A}_{8,n}$ , and  $\overline{A}_{9,n}$  are as follows (the others are also time-independent coefficients and are not presented in this study because they are not of interest in this study):

$$\overline{\overline{A}}_{6,n} = \frac{-S_n \omega_{b,n}^2}{2\sqrt{1 - \varepsilon_{b,n}^2}} \left\{ \frac{\mu_n (1 + S_n)^3 + \varepsilon_{b,n}^2 \mu_n (1 + S_n) + (1 + S_n)^2 - \varepsilon_{b,n}^2}{\left[ \left(\mu_n (1 + S_n) + 1\right)^2 + \varepsilon_{b,n}^2 \mu_n^2 \right]} + \frac{-\mu_n (1 + S_n)^3 - \varepsilon_{b,n}^2 \mu_n (1 + S_n) + (1 + S_n)^2 - \varepsilon_{b,n}^2}{\left[ \left(\mu_n (1 + S_n) - 1\right)^2 + \varepsilon_{b,n}^2 \mu_n^2 \right]} \right\}$$
(18)

$$\overline{\overline{A}}_{7,n} = \frac{-S_n \omega_{b,n}^2}{2\sqrt{1 - \varepsilon_{b,n}^2}} \left\{ \frac{-\mu_n (1 - S_n)^3 - \varepsilon_{b,n}^2 \mu_n (1 - S_n) - (1 - S_n)^2 + \varepsilon_{b,n}^2}{\left[ \left(\mu_n (1 - S_n) + 1\right)^2 + \varepsilon_{b,n}^2 \mu_n^2 \right]} + \frac{\mu_n (1 - S_n)^3 + \varepsilon_{b,n}^2 \mu_n (1 - S_n) - (1 - S_n)^2 + \varepsilon_{b,n}^2}{\left[ \left(\mu_n (1 - S_n) - 1\right)^2 + \varepsilon_{b,n}^2 \mu_n^2 \right]} \right\}$$
(19)

$$\overline{\overline{A}}_{8,n} = \frac{-S_n \omega_{b,n}^2 \varepsilon_{b,n}}{2\sqrt{1 - \varepsilon_{b,n}^2}} \left\{ \frac{-\mu_n (1 + S_n)^2 - \varepsilon_{b,n}^2 \mu_n - 2(1 + S_n)}{\left[\left(\mu_n (1 + S_n) + 1\right)^2 + \varepsilon_{b,n}^2 \mu_n^2\right]} + \frac{\mu_n (1 + S_n)^2 + \varepsilon_{b,n}^2 \mu_n - 2(1 + S_n)}{\left[\left(\mu_n (1 + S_n) - 1\right)^2 + \varepsilon_{b,n}^2 \mu_n^2\right]} \right\}$$
(20)

$$\overline{\overline{A}}_{9,n} = \frac{-S_n \omega_{b,n}^2 \varepsilon_{b,n}}{2\sqrt{1 - \varepsilon_{b,n}^2}} \left\{ \frac{\mu_n (1 - S_n)^2 + \varepsilon_{b,n}^2 \mu_n + 2(1 - S_n)}{\left[ \left( \mu_n (1 - S_n) + 1 \right)^2 + \varepsilon_{b,n}^2 \mu_n^2 \right]} + \frac{-\mu_n (1 - S_n)^2 - \varepsilon_{b,n}^2 \mu_n + 2(1 - S_n)}{\left[ \left( \mu_n (1 - S_n) - 1 \right)^2 + \varepsilon_{b,n}^2 \mu_n^2 \right]} \right\}$$
(21)

and

$$\mu_n = \frac{\omega_{b,n}}{\omega_v} \tag{22}$$

To successfully identify the mode shape of a bridge, the component response corresponding to the frequency of the *n*th bridge mode should be singled out from the vehicle accelerations, which is feasible by implementing an appropriate signal processing tool, such as the band-pass filters or singular spectrum analysis (Yang et al. 2014). In this way, the extracted bridge component response associated with the *n*th mode is

$$R_{b} = e^{-\varepsilon_{b,n}\omega_{b,n}t} \left[ \overline{\overline{A}}_{6,n}\cos\left(\omega_{b,n}t + \frac{n\pi\nu t}{L} - \beta\right) + \overline{\overline{A}}_{7,n}\cos\left(\omega_{b,n}t - \frac{n\pi\nu t}{L} - \beta\right) + \overline{\overline{A}}_{8,n}\sin(\omega_{b,n}t + n\pi\nu t/L - \beta) + \overline{\overline{A}}_{9,n}\sin(\omega_{b,n}t - n\pi\nu t/L - \beta) \right]$$

$$(23)$$

Then this extracted  $R_b$  is processed by the HT to yield its transform pair

$$\widehat{R}_{b} = e^{-\varepsilon_{b,n}\omega_{b,n}t} \left[ \overline{\overline{A}}_{6.n} \sin\left(\omega_{b,n}t + \frac{n\pi\nu t}{L} - \beta\right) + \overline{\overline{A}}_{7.n} \sin\left(\omega_{b,n}t - \frac{n\pi\nu t}{L} - \beta\right) - \overline{\overline{A}}_{8.n} \sin\left(\omega_{b,n}t + \frac{n\pi\nu t}{L} - \beta\right) - \overline{\overline{A}}_{9.n} \sin\left(\omega_{b,n}t - n\pi\nu t/L - \beta\right) \right]$$
(24)

If the vehicle moves slowly enough, the driving frequency  $n\pi v/L$  is regarded as much less than the bridge frequency  $\omega_{b,n}$ , i.e.,  $S_n \ll 1$ . Accordingly, the coefficients of  $R_b$  and  $\widehat{R}_b$  reduce to the following:

$$\overline{\overline{A}}_{6,n} = -\overline{\overline{A}}_{7,n} = \frac{-S_n \omega_{b,n}^2}{2\sqrt{1 - \varepsilon_{b,n}^2}} \times \left\{ \frac{\mu_n + \varepsilon_{b,n}^2 \mu_n + 1 - \varepsilon_{b,n}^2}{\left[ (\mu_n + 1)^2 + \varepsilon_{b,n}^2 \mu_n^2 \right]} + \frac{-\mu_n - \varepsilon_{b,n}^2 \mu_n + 1 - \varepsilon_{b,n}^2}{\left[ (\mu_n - 1)^2 + \varepsilon_{b,n}^2 \mu_n^2 \right]} \right\}$$
(25)

$$\overline{\overline{A}}_{8,n} = -\overline{\overline{A}}_{9,n} = \frac{-S_n \omega_{b,n}^2 \varepsilon_{b,n}}{2\sqrt{1 - \varepsilon_{b,n}^2}} \times \left\{ \frac{-\mu_n - \varepsilon_{b,n}^2 \mu_n - 2}{\left[(\mu_n + 1)^2 + \varepsilon_{b,n}^2 \mu_n^2\right]} + \frac{\mu_n + \varepsilon_{b,n}^2 \mu_n - 2}{\left[(\mu_n - 1)^2 + \varepsilon_{b,n}^2 \mu_n^2\right]} \right\}$$
(26)

Therefore, from Eq. (3), the instantaneous amplitude of  $R_b$  can be obtained as

$$A(t) = \sqrt{R_b^2(t) + \widehat{R}_b^2(t)} = 2\sqrt{\overline{A}_{6,n}^2 + \overline{A}_{8,n}^2} e^{-\varepsilon_{b,n}\omega_{b,n}t} \left| \sin \frac{n\pi vt}{L} \right|$$
(27)

Replacing x with vt in Eq. (27) yields

$$A\left(\frac{x}{v}\right) = \sqrt{R_b^2(t) + \widehat{R}_b^2(t)} = 2\sqrt{\overline{A}_{6,n}^2 + \overline{\overline{A}}_{8,n}^2} e^{-\varepsilon_{b,n}\omega_{b,n}x/v} \left| \sin\frac{n\pi x}{L} \right|$$
(28)

Compared with Yang et al. (2014), Eq. (28) shows that the amplitude history A(x/v) of the extracted component response includes the mode shape function  $\sin n\pi x/L$  of the bridge (in absolute value) multiplied by a constant nontime (or position)-related coefficient,  $2\sqrt{\overline{A}_{6,n}^2 + \overline{A}_{8,n}^2}$ . However, the bridge damping is observed to shift the mode shape in the amplitude history. The following numerical study will provide evidence that the mode shape shift caused by bridge damping is nonnegligible. Therefore, the construction of the mode shape from the amplitude of HT needs to be reformulated as  $A_{\text{mod},n} = A(x/v)/e^{-\varepsilon_{b,n}\omega_{b,n}x/v}$  and its normalization, which is feasible when the speed of the test vehicle is constant.

## Algorithm

In the theoretical derivation, there is a significant assumption that the vehicle mass is negligible compared with the bridge mass. In addition, the most important point of the proposed algorithm is to keep the vehicle speed as low and constant as possible. Its effect on accuracy will be investigated through numerical simulation in the following. Based on the previously mentioned derivation, the procedural steps for identifying the bridge modal parameters using a passing vehicle response are as follows (Fig. 2):

- 1. Record the axle acceleration, R(t), during its passage over the bridge.
- 2. Identify the bridge natural frequencies  $\omega_{b,n}$  from the recorded signal R(t); this step can be performed using signal processing techniques, such as Fourier transform (McGetrick et al. 2009;

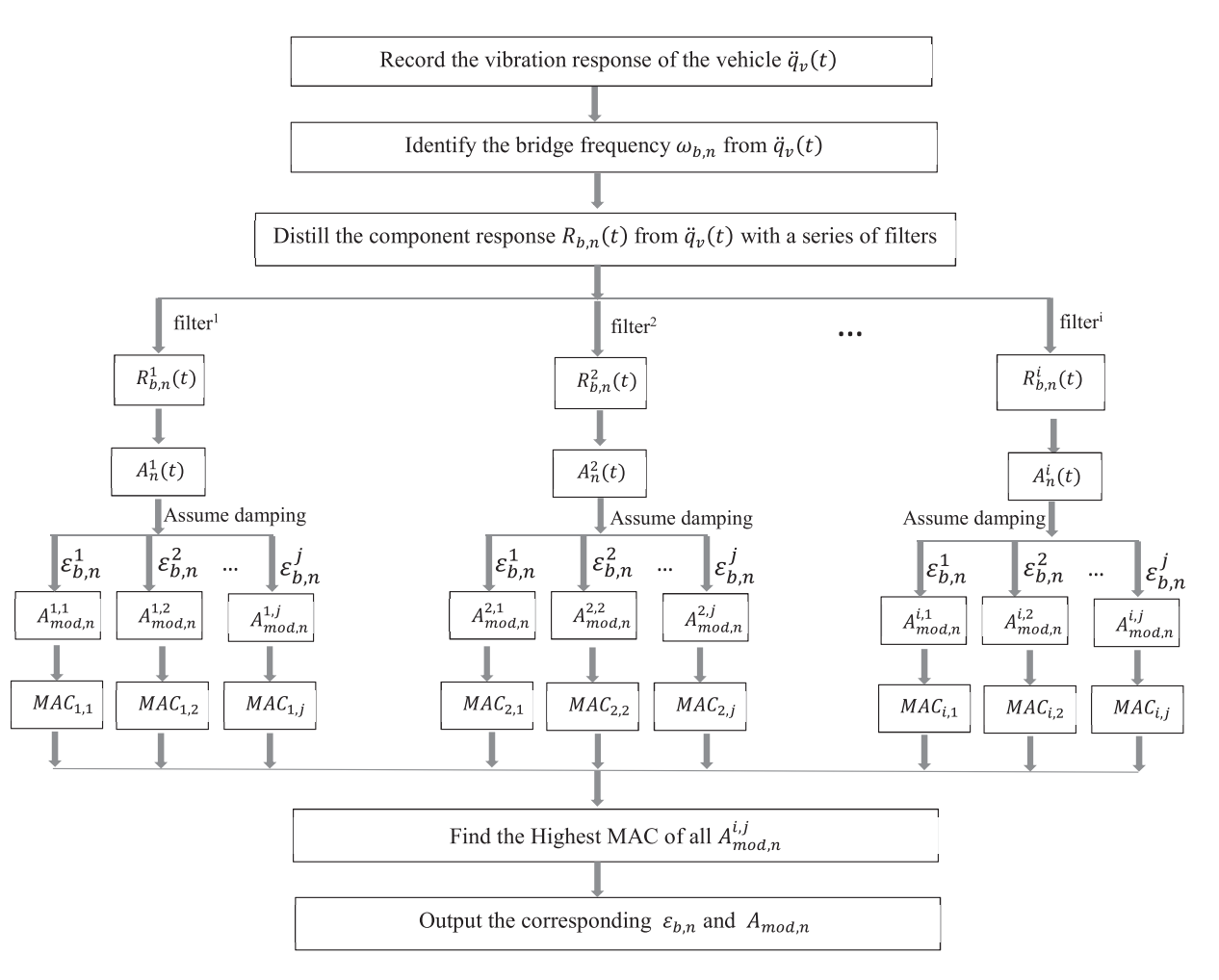


Fig. 2. Flowchart. MAC = modal assurance criteria.

Yang et al. 2014; Yang and Lin 2005) or wavelet transform (Tan et al. 2017).

3. Single out the component response associated with a bridge natural frequency from R(t). Principally, with known frequency,  $\omega_{b,n}$ , the component response  $R_{b,n}(t)$  associated with  $\omega_{b,n}$  can be extracted with standard signal processing tools, such as band-pass filtering or singular spectrum analysis. A band-pass filter is applied in this study. In practice, selecting a suitable filter and obtaining the optimum  $R_{b,n}(t)$  is another challenge. In this study, the parameters are varied to overcome it. In a 3-dB bandwidth band-pass filter, the parameters of the central frequency,  $f_c$ , and the quality factor, Q, determine the filter. The lower and upper cutoff frequencies are represented by

$$f_l = f_c \left( \sqrt{1 + \frac{1}{4Q^2}} - \frac{1}{2Q} \right) \text{ and } f_u = f_c \left( \sqrt{1 + \frac{1}{4Q^2}} + \frac{1}{2Q} \right)$$

respectively. It is noted that a low Q factor gives a broad (wide) bandwidth, whereas a high Q factor gives a narrow (small) bandwidth. By changing the values of  $f_c$  and Q, the component response,  $R_{b,n}(t)$ , is found.

4. From these responses,  $R_{b,n}(t)$ , the HT is computed to yield  $\widehat{R}_{b,n}(t)$ , and then a series of instantaneous amplitudes,  $A_n(t)$ , are calculated.

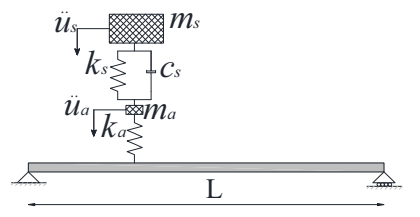


Fig. 3. VBI model used in simulations.

- 5. Assuming a series of damping ratios  $\varepsilon_{b,n}$  each amplitude function is adjusted as  $A(x/v)/e^{-\varepsilon_{b,n}\omega_{b,n}x/v}$  and normalized to find the mode shapes  $A_{\text{mod},n}$ .
- 6. Calculate the modal assurance criteria (MAC) of the achieved  $A_{\text{mod},n}$  values and compare with the theoretical mode shapes.
- 7. The value of  $A_{\text{mod},n}$  with the highest MAC is the bridge mode shape. For all  $R_{b,n}(t)$  and  $\varepsilon_{b,n}$ , identify the maximum MAC and, hence, the final  $A_{\text{mod},n}$  and bridge damping ratio.

## **Numerical Simulation**

To verify the feasibility of extracting the damping ratio and mode shapes of a bridge from a passing vehicle, a quarter-car VBI model is adopted, as given in Fig. 3. The road surface profile is not considered at first (it is considered in the following case study) and the

Table 1. Vehicle and bridge properties

| Property                   | Value                               |
|----------------------------|-------------------------------------|
| Vehicle                    |                                     |
| $m_{\scriptscriptstyle S}$ | 14,000 kg                           |
| $k_s$                      | 200 kN/m                            |
| $c_s$                      | 10 kN s/m                           |
| $m_a$                      | 1,000 kg                            |
| $k_a$                      | 2,750 kN/m                          |
| Bridge                     |                                     |
| Span                       | 25 m                                |
| Density                    | $4,800 \text{ kg/m}^3$              |
| Width                      | 4 m                                 |
| Depth                      | 0.8 m                               |
| Modulus                    | $2.75 \times 10^{10} \text{ N/m}^2$ |

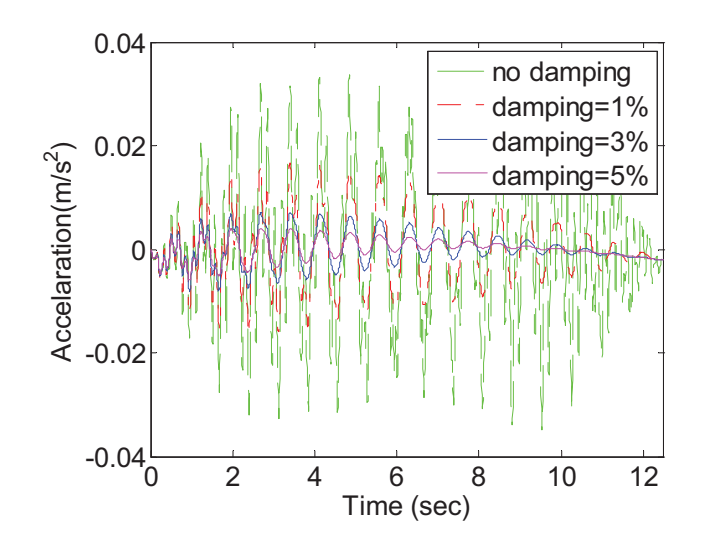
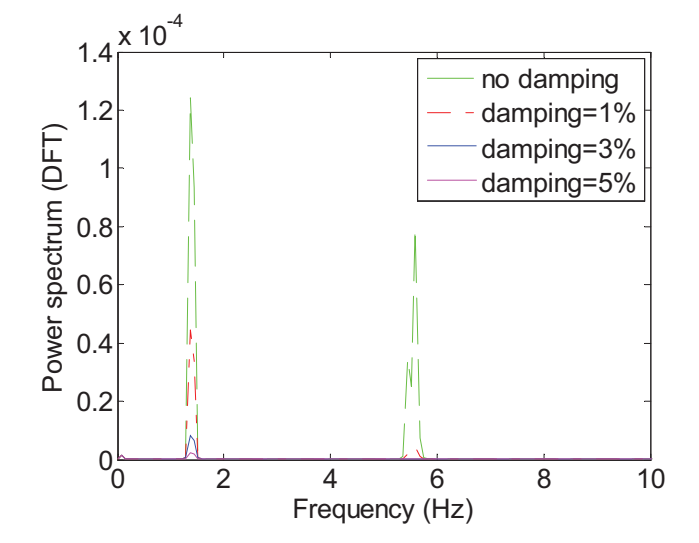
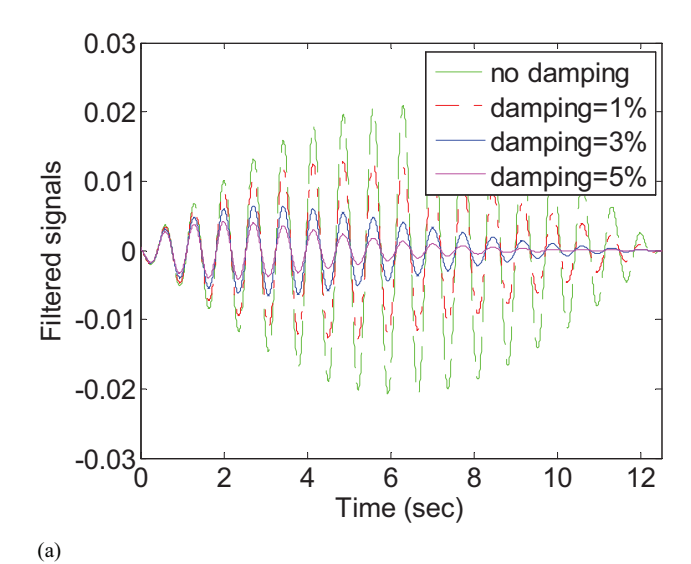
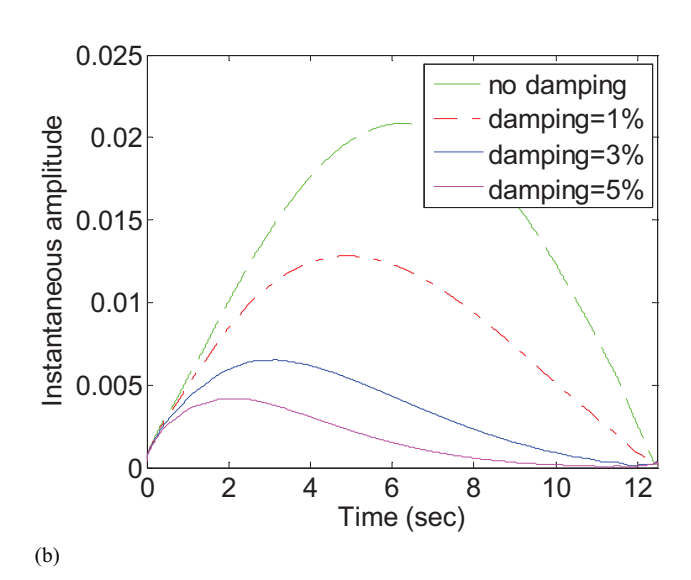


Fig. 4. Vehicle acceleration responses.



**Fig. 5.** Spectrum of accelerations. DFT= discrete Fourier transform.





**Fig. 6.** (a) Filtered signals; and (b) instantaneous amplitude.

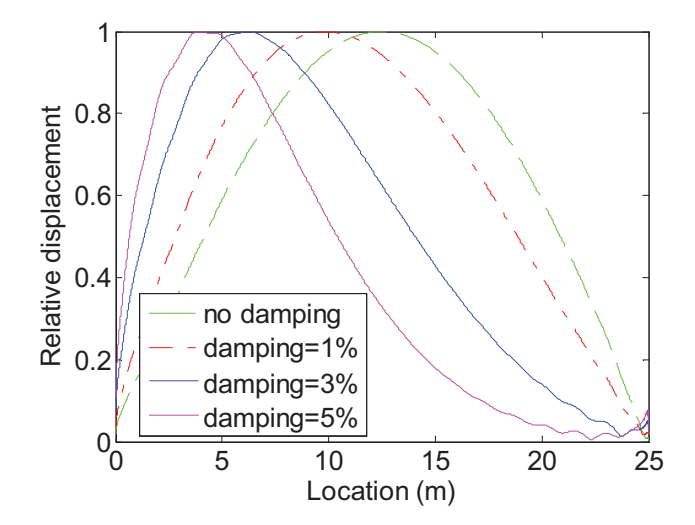
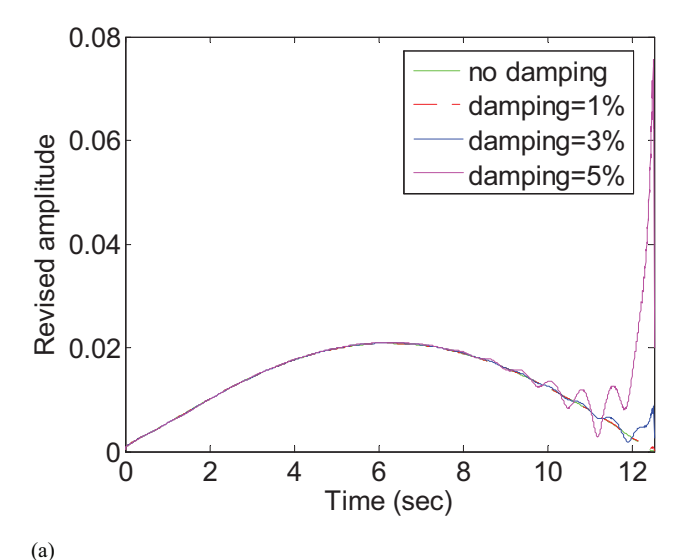
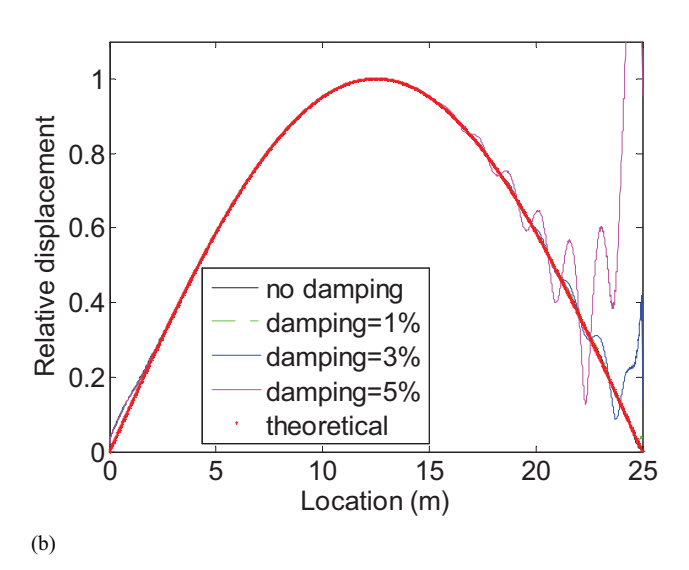


Fig. 7. Noncorrected results of extracted mode shape.





**Fig. 8.** (a) Revised instantaneous amplitude, A(t); and (b) normalized  $A_{\text{mod}}$  of the bridge.

vehicle is assumed to travel at constant speed. The vehicle and bridge properties, listed in Table 1, are based on the recommendations of Cebon (1999) and Yang and Lee (2018). As shown in the proposed algorithm, it is necessary to identify the bridge frequencies from the vehicle response. However, Yang and Lee (2018) pointed out that vehicle damping that is too high tends to make the bridge frequencies invisible in the vehicle's spectra. They also showed that vehicle damping can improve the identification of the first bridge frequency from the vehicle's spectra, considering the road surface roughness. To identify the bridge frequency successfully, from the passing vehicle response, a typical vehicle damping is adopted in this study. The dynamic interaction between the vehicle and the bridge is modeled in MATLAB. Except where otherwise mentioned, the scanning frequency used is 200 Hz. The first two natural frequencies of the bridge,  $f_b$ , are 1.39 and 5.56 Hz. The vehicle frequencies are 0.58 and 8.65 Hz.

# Effect of Bridge Damping: Exacting Damping Ratio and Mode Shapes

Fig. 4 illustrates the vehicle acceleration responses resulting from bridge damping for four scenarios: no damping, 1% (bridge) damping ratio, 3% damping ratio, and 5% damping ratio. Rayleigh damping is applied in each case. To possess enough speed for the theoretical analysis, a vehicle speed of 2 m/s is adopted in this case, as suggested by Yang et al. (2014). These responses are processed by the fast Fourier transform to yield the frequency spectrum, as presented in Fig. 5. The first identified frequency, at approximately 1.38 Hz, can be recognized as the first bridge frequency. Using band-pass filters, the component responses corresponding to the first identified bridge frequency are decomposed from the accelerations, as given in Fig. 6(a). The HT is applied to these filtered signals to yield the instantaneous amplitudes, A(t), as illustrated in Fig. 6(b).

The separated component without damping oscillates with varying amplitudes that are similar to the first mode shape of the bridge. Consequently, its instantaneous amplitude A(t) is quite close to the theoretical first mode shape of the bridge. However, it is observed that the bridge damping shrinks and shifts the instantaneous amplitude, A(t), when compared with the case without damping. The results based on the algorithm presented by Yang et al. (2014),

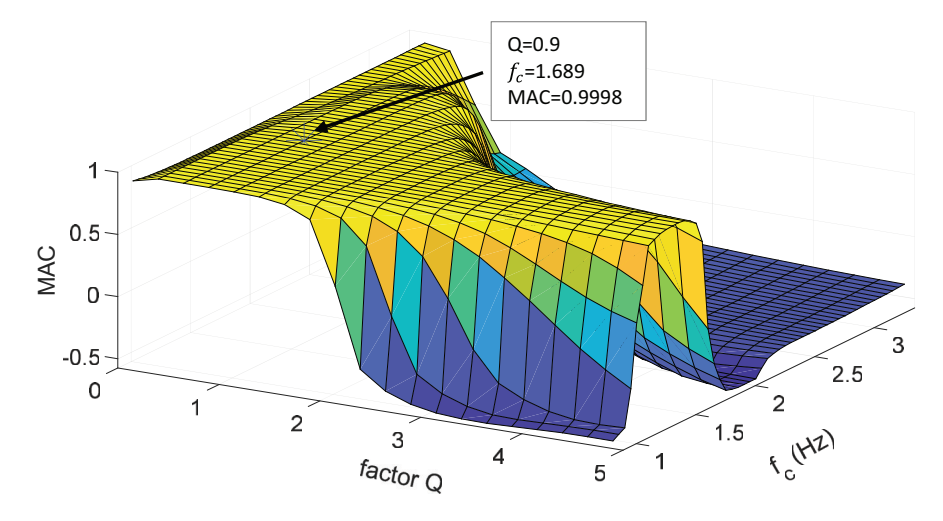
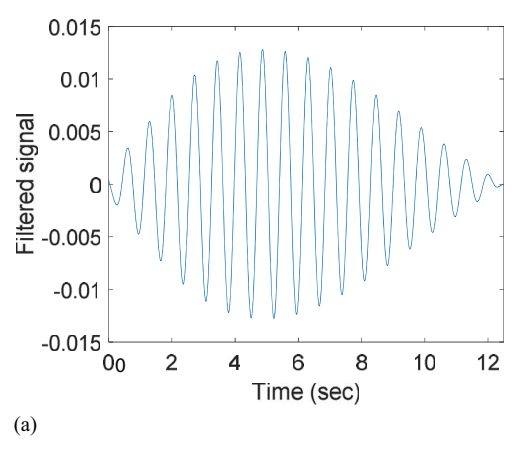
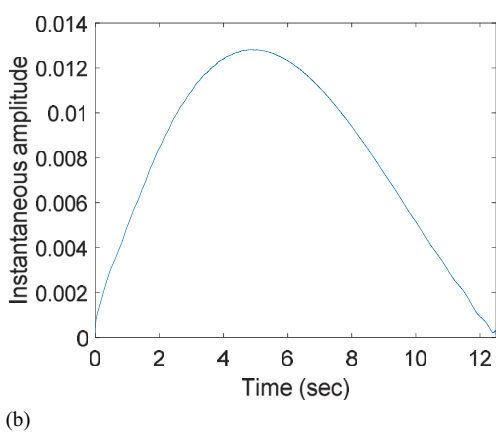


Fig. 9. Maximum values of MAC for each assumed parameter pair in the band-pass filter.

which ignores the bridge damping and uses the normalized instantaneous amplitude of HT associated with the filtered signal to represent the bridge mode shape directly, are illustrated in Fig. 7. They are referred to as the noncorrected mode shape in this study.

Results have shown that the bridge damping apparently left shifts the extracted mode shape, which causes a greater error on the construction of the bridge mode shape with HT, although the value of the damping ratio is as small as 1%. The instantaneous amplitude with damping is revised with  $A(t)/e^{-\varepsilon_{b,n}\omega_{b,n}t}$ , and the results are given in Fig. 8(a). These revised instantaneous amplitudes are extremely close to those without damping, and they confirm the





**Fig. 10.** (a) Filtered signal of vehicle response; and (b) corresponding instantaneous amplitude.

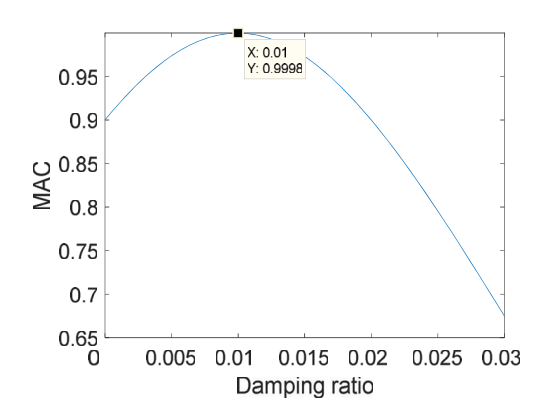


**Fig. 11.** Variation of MAC value with damping ratio. Highest MAC corresponds to actual damping.

theoretical analysis, indicating that this process can remove the damping effect on the mode shape extracted with HT. Therefore, the proposed algorithm, referred to as the corrected approach, can improve to extract the bridge mode shape from a passing vehicle acceleration when bridge damping exists. These revised instantaneous amplitudes are normalized in Fig. 8(b) and represent the bridge mode shape.

However, the higher bridge damping ratio generates a stronger edge effect, as illustrated in Fig. 8, which negatively affects accuracy of the proposed algorithm on the mode shape construction and damping ratio identification. This edge effect happens because the end section of instantaneous amplitude, A(t), is not smooth enough when the damping ratio is higher, and the revising process best amplifies this section. To overcome it, one can appropriately smooth the instantaneous amplitude, A(t), before revising it.

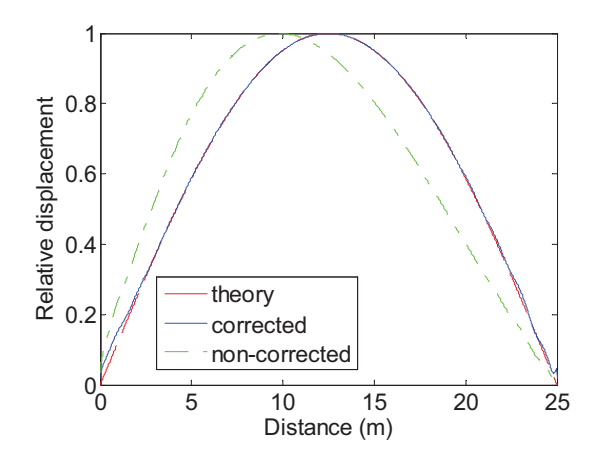
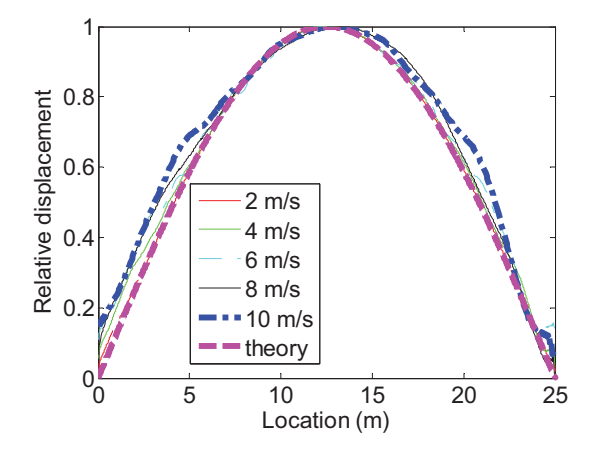


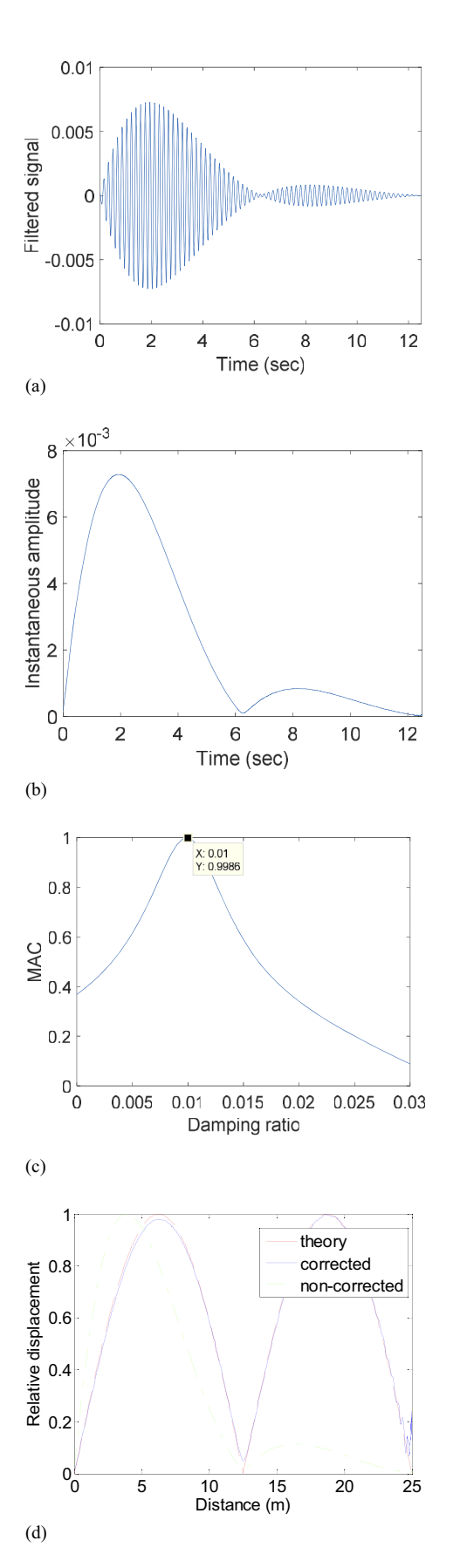
Fig. 12. Extracted first mode shape of the bridge.

Table 2. Extracted damping for different vehicle speeds

| Speed (m/s) | Damping ratio | Error (%) | MAC    |
|-------------|---------------|-----------|--------|
| 2           | 0.0100        | 0         | 0.9998 |
| 4           | 0.0100        | 0         | 0.9989 |
| 6           | 0.0105        | -5        | 0.9968 |
| 8           | 0.0160        | -60       | 0.9939 |
| 10          | 0.0225        | -125      | 0.9914 |



**Fig. 13.** Extracted first mode shape of the bridge for different vehicle speeds.



**Fig. 14.** Bridge higher modal parameters identification: (a) signal after suitable filtering; (b) amplitude of HT; (c) damping ratio versus MAC; and (d) extracted mode shape.

Otherwise, the strong edge-effect section should not be involved in calculating the MAC.

This section applies the steps described previously to extract the bridge damping ratio and mode shape. The same case with a damping ratio of 1% is considered. A wide range of band-pass filter parameters are considered; central frequency,  $f_c$ , ranges from 0.789 to 3.239 Hz in steps of 0.01 Hz, and the factor Q ranges from 0.15 to 4.9 in steps of 0.25. For each  $f_c$  and Q, following Steps 3 and 4 of the proposed algorithm, a series of instantaneous amplitudes, f(t), is obtained. The corrected function,  $f(t)/e^{-\varepsilon_{b,n}\omega_{b,n}t}$ , is applied in all

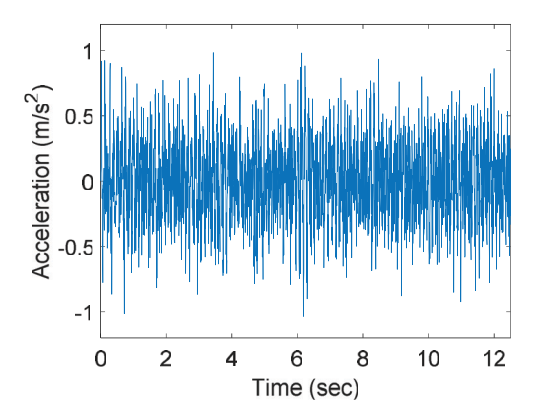


**Fig. 15.** Recorded vehicle response at road roughness.

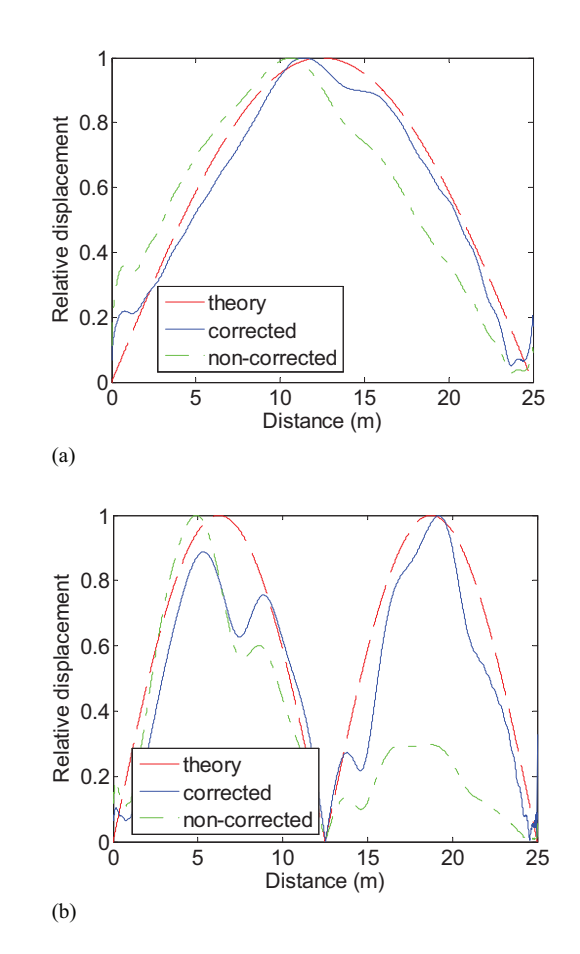


**Fig. 16.** Extracted mode shapes of the bridge: (a) first mode shape; and (b) second mode shape.

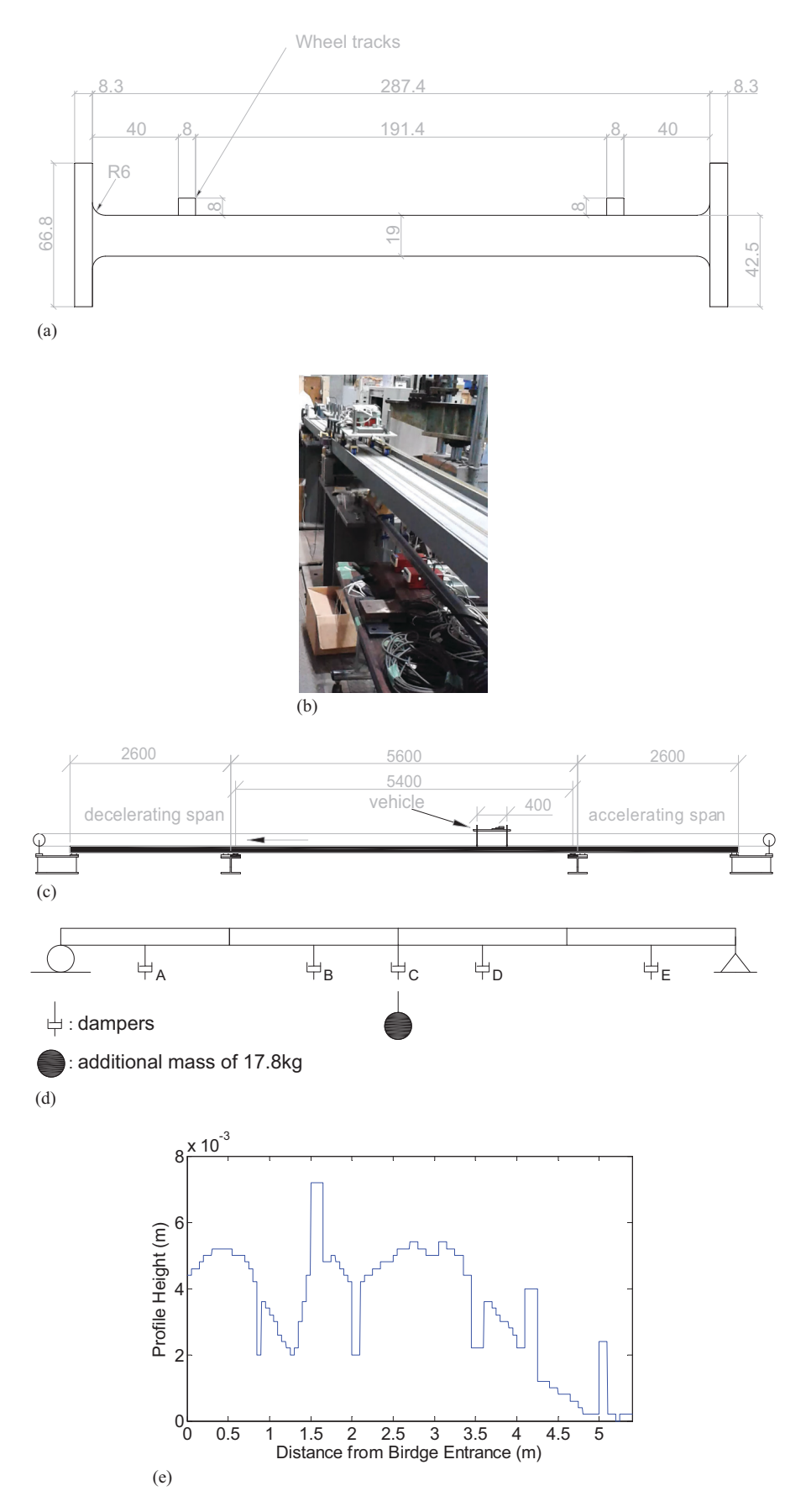


**Fig. 17.** Experimental bridge: (a) beam cross section (unit: millimeters); (b) elevation of setup; (c) laboratory setup (unit: millimeters); (d) experimental setup for changing damping ratio; and (e) experimental road profile.

cases, assuming a damping ratio ranging from 0 to 0.03 in steps of 0.0005, to create  $M_{\rm odal}$  and then normalize it. For each  $(Q, f_c)$  pair, only one record for the maximum MAC results in these assumed damping ratios. The results for all parameter pairs are illustrated in Fig. 9. As shown, the maximum MAC happens when  $f_c = 1.689$  Hz and Q = 0.9, implying lower and upper cutoff frequencies of 0.994 and 2.871 Hz, respectively. For this band-pass filter, the component R(t) associated with the first bridge frequency is decomposed, as presented in Fig. 10(a), and the corresponding instantaneous amplitude is as illustrated in Fig. 10(b).

This instantaneous amplitude is applied to the function  $A(t)/e^{-\varepsilon_{b,n}\omega_{b,n}t}$  to remove the effect of damping and to obtain  $A_{\rm mod}$  for each assumed damping ratio. Each value of  $A_{\rm mod}$ , for every damping ratio, yields a MAC that is compared with the theoretical one, as illustrated in Fig. 11. When the damping ratio equals the actual value of 1%, the highest MAC value occurs. The extracted mode shape, with a very high MAC value of 0.9998, is given in Fig. 12 and compares very well with the theoretical one. In addition, Fig. 12 demonstrates a great improvement of the extracted mode shape with the proposed algorithm compared with that of the noncorrected one.

# Effect of Vehicle Speed

The effect of the vehicle speed on the proposed algorithm is studied, considering five different vehicle speeds: v = 2, 4, 6, 8, and 10 m/s. The remaining properties of the VBI model are kept the same as previously mentioned. Following the same procedure, the mode shape and damping ratio are identified for each vehicle speed and presented in Table 2. The extracted mode shapes of the bridge are given in Fig. 13. The effect of vehicle speed on the identified results can be clearly seen in Table 2 and Fig. 13.

When the vehicle speed is slow (2 m/s or 4 m/s), the constructed mode shape and identified damping ratio match very well with the actual ones. As vehicle speed increases, the errors in both damping ratio and mode shape become greater. When the vehicle is 10 m/s, the error is as high as 125%. This finding is consistent with the theoretical analysis and studies of Malekjafarian and Obrien (2014) and Yang et al. (2014).

#### Case Study of Higher Mode Shape

This section investigates the extraction of a higher mode shape and associated damping ratio. The vehicle acceleration of Fig. 4, with a damping ratio of 1%, is considered (vehicle speed = 2 m/s; without road roughness). As previously mentioned, the optimum band-pass filter is first found and applied to obtain the component response associated with the second frequency of the bridge, as illustrated in Fig. 14(a). The corresponding instantaneous amplitude of the HT can also be obtained and is given in Fig. 14(b). Clearly, the damping ratio has a greater effect on the higher mode shape amplitude than on the first mode shape. Nevertheless, the proposed algorithm can accurately identify the damping ratio as 0.01 and the second mode shape of the bridge with a high MAC of 0.9986. The extracted results are given in Figs. 14(c and d).

# Effect of Road Surface Roughness

The effect of road surface roughness is investigated in this section. The road profile is generated randomly according to the PSD curve of a "class A" profile, as described in ISO 8608 (ISO 1995). Fig. 15 illustrates the vehicle acceleration response considering the generated road roughness when the vehicle velocity is 2 m/s. Following the process described previously, the mode shapes associated with

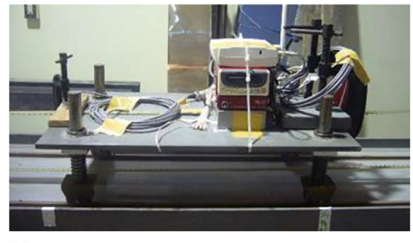
the first two natural frequencies of the bridge are extracted and are presented in Fig. 16. In this case, for the first mode shape of the bridge, the damping ratio and MAC value are calculated as 0.011 (10% error) and 0.9878, respectively. For the second mode shape, the damping ratio and MAC value are calculated as 0.005 (50% error) and 0.9060, respectively. Although the band-pass filter can partially remove the random vibration caused by road roughness, the roughness has a negative impact on the proposed algorithm, especially for the higher modes. Because the road profile injects a wide range of spatial frequencies into the vehicle acceleration, the road roughness effect cannot be removed completely from the extracted mode shapes using a frequency-domain filtering technique (Yang and Lee 2018; Yang et al. 2014). Note that the extracted higher modes are more sensitive to road roughness because of their relatively lower amplitudes (Yang et al. 2014).

# **Laboratory Studies**

A scaled moving vehicle laboratory experiment is performed to investigate the feasibility of using indirect measurement to monitor bridge health. The scaled bridge model used in the experiment is summarized in Fig. 17. Two approach spans are used for vehicle acceleration and deceleration. The main span is a 5.4-m simply supported steel beam. The beam properties, obtained from the manufacturer and free vibration tests, are listed in Table 3. The road surface roughness is also considered in the experiment, as illustrated in Fig. 17(e). This road profile was scaled using an electrical tape to pave on both wheel paths of the test vehicle at the interval of

Table 3. Structural properties of model girder

| Property                                       | Value                 |  |  |
|--|-----------------------|--|--|
| Span length [L (m)]                            | 5.4                   |  |  |
| Material density (kg/m <sup>3</sup> )          | 7,800                 |  |  |
| Cross-sectional area [A (m <sup>2</sup> )]     | $6.7 \times 10^{-3}$  |  |  |
| First natural frequency (Hz)                   | 2.69                  |  |  |
| Damping ratio for first mode ( $\varepsilon$ ) | 0.016                 |  |  |
| Second moment of area (m <sup>4</sup> )        | $5.77 \times 10^{-7}$ |  |  |



(a)



**Fig. 18.** Experimental vehicle: (a) side view; and (b) end view showing sensors.

100 mm based on a real road profile measured on a 40.4-m road bridge in Japan (Kim et al. 2005), which was categorized as very good (Class A) according to ISO 8608 (ISO 1995). This road profile is intended to be representative of that expected on a typical highway bridge. However, there are some discrepancies with the measured profile because the scaled road profile as a superposition of steps is formed by a simple construction method using layered tape and plastic strips (McGetrick et al. 2015).

The damping of the test beam was varied in this experiment, and it can be categorized in three scenarios: Scenario 1, no change to the test beam; Scenario 2, applying old displacement transducer at Point C on the bridge; and Scenario 3, applying old displacement transducers at Points A–E and a mass of 17.8 kg at midspan, as given in Fig. 17(d). The old transducers are used because they provide frictional resistance to bridge displacements at the chosen locations. The damping constant changes from 1.6% for the initial case to 2.1% and 4.3% because of an additional damper at midspan and five additional dampers, respectively. The additional mass is

Table 4. Vehicle model properties

| Axle | Mass<br>(kg) | Suspension stiffness (N/m) | Suspension damping $(N \cdot s/m)$ |
|------|--------------|----------------------------|------------------------------------|
| 1    | 7.9          | 2,680                      | 16.006                             |
| 2    | 13.445       | 4,570                      | 27.762                             |

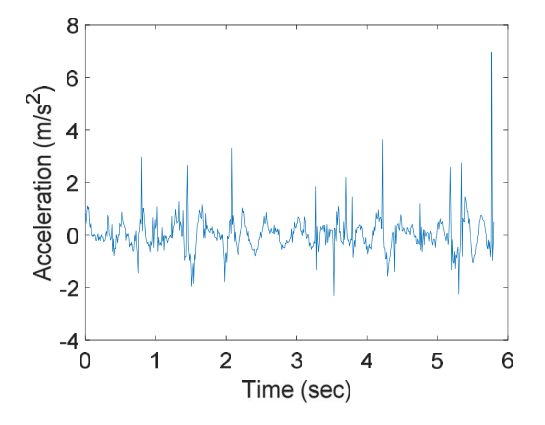


Fig. 19. Rear axle acceleration

performed to adjust the bridge frequency as frequently damaged, which causes changes in damping that may cause some change in frequency. The additional mass brings about the first natural frequency drop of the bridge from 2.69 to 2.50 Hz.

A scaled two-axle vehicle model is instrumented for the experiments, as illustrated in Fig. 18. Two accelerometers are mounted on the center of the front and rear axles, respectively, to monitor the vehicle bounce motion. This instrumented vehicle also includes a wireless router and data logger, which allow the axle acceleration data to be recorded remotely. The vehicle model configurations are given in Table 4. The axle spacing and track width are 0.4 and 0.2 m, respectively.

The test vehicle was propelled by a motor and pulley system. Its speed, therefore, was maintained constant by an electronic controller as it passed over the bridge. The entry and exit of the vehicle to the beam were monitored using strain sensors to synchronize measurements; entry and exit points appeared as peaks in the strain signals. The instrumented vehicle speed was 0.93 m/s in this experiment. The vehicle repeatedly crossed the bridge (five times for each scenario) at this speed. More details of this experiment are given in Kim et al. (2011, 2014) and McGetrick et al. (2015).

In this experiment, extracting the frequency of the bridge using the acceleration signal measured on the vehicle was well investigated and is presented by Kim et al. (2011, 2014). This study focuses on the extraction of the damping ratio and mode shape of the bridge from the vehicle response. The unsprung acceleration was recorded on the rear axle of the vehicle.

Fig. 19 illustrates one of five recorded vehicle acceleration signals during its passage over the bridge in Scenario 1 (time 0 is when it entered the bridge; the end time is when it left the bridge). Following the described algorithm, a series of parameters for the band-pass filter and damping ratios are assumed. At these assumed values, the highest MAC of the first mode shape is found when  $f_c = 2.44$  Hz and Q = 4.5, which gives a damping ratio of 0.0165. The values of MAC for each assumed parameter pair of the band-pass filter are plotted in Fig. 20. The results for this maximum MAC are given in Fig. 21. The bridge damping ratio is identified as 0.0165 (compared with the actual value of 0.016). The extracted mode shape is also good with a high MAC of 0.9933. In addition, the proposed algorithm demonstrates that the extraction of mode shape is greatly improved compared with the noncorrected results.

Similarly, applying the proposed algorithm to all of the recorded accelerations, the extracted damping ratios and MAC values are listed in Table 5. As illustrated, the extracted mode shapes match

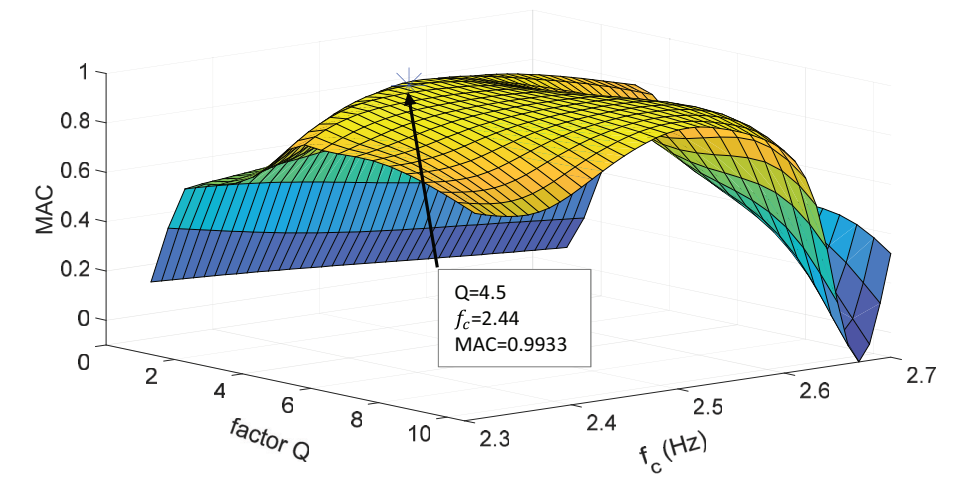


**Fig. 20.** MAC versus parameters of band-pass filter.

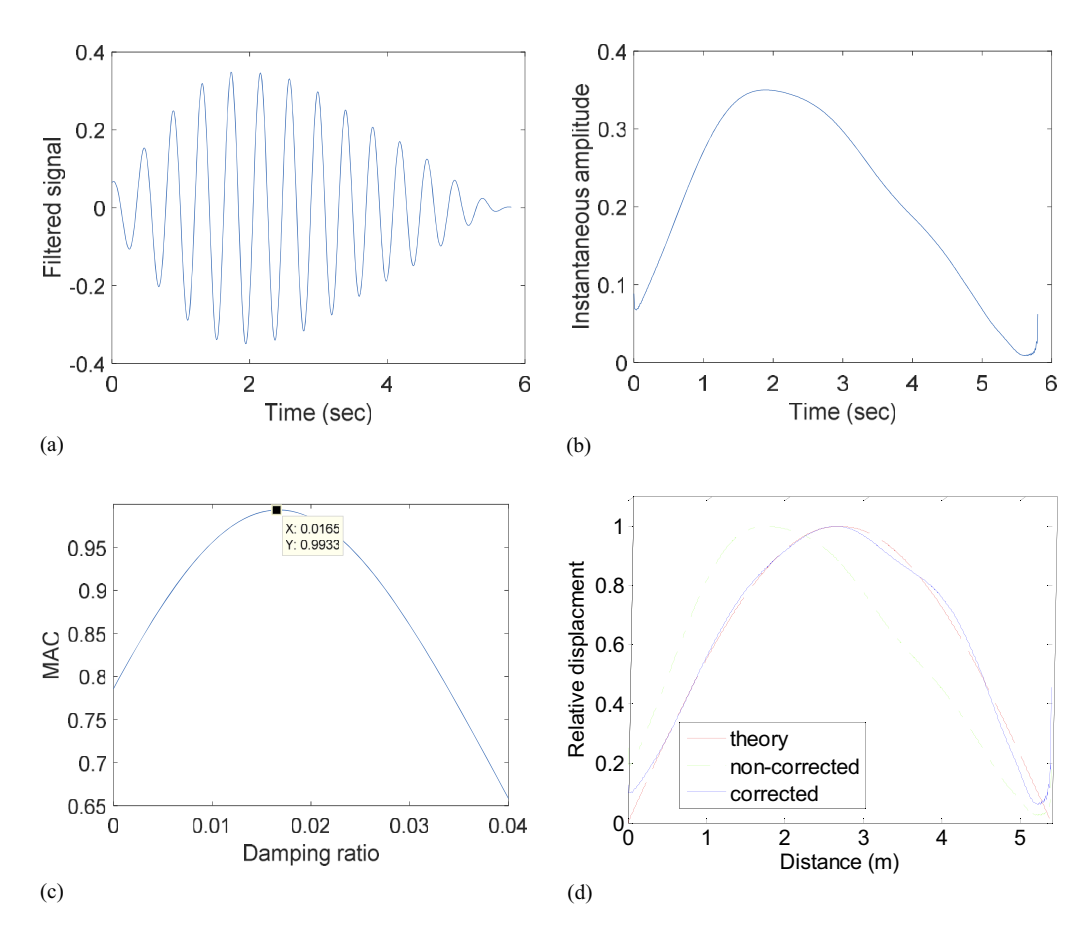


Fig. 21. Extraction of mode shape for Test no. 1, Scenario 1: (a) filtered signal; (b) corresponding instantaneous amplitude of HT; (c) damping ratio versus MAC; and (d) extracted mode shape.

**Table 5.** Extracted results for three scenarios with different damping ratios,  $\varepsilon$ 

|  |                  | Test no. |        |        |        |        |                    |                    |
|--|------------------|----------|--------|--------|--------|--------|--------------------|--------------------|
| Scenario                                 | Extracted result | 1        | 2      | 3      | 4      | 5      | Mean of five tests | Standard deviation |
| Scenario 1 ( $\varepsilon$ = 0.016)      | Damping ratio    | 0.0165   | 0.0165 | 0.0145 | 0.0135 | 0.0155 | 0.0155             | 0.0014             |
|  | MAC              | 0.9933   | 0.9903 | 0.9871 | 0.9945 | 0.9899 | 0.9910             | 0.0029             |
| Scenario 2 ( $\varepsilon = 0.021$ )     | Damping ratio    | 0.0200   | 0.0225 | 0.0185 | 0.0180 | 0.0215 | 0.0201             | 0.0019             |
|  | MAC              | 0.9768   | 0.9310 | 0.9639 | 0.9812 | 0.9454 | 0.9597             | 0.0212             |
| Scenario 3 ( $\varepsilon = 0.043$ )     | Damping ratio    | 0.0285   | 0.0305 | 0.015  | 0.031  | 0.0315 | 0.0270             | 0.0070             |
|  | MAC              | 0.9725   | 0.9650 | 0.9937 | 0.9710 | 0.9546 | 0.9711             | 0.0143             |
| Scenario $3^*$ ( $\varepsilon = 0.043$ ) | Damping ratio    | 0.0415   | 0.0420 | _      | 0.0430 | 0.0420 | 0.0421             | 0.0006             |
|  | MAC              | 0.9939   | 0.9924 | _      | 0.9934 | 0.9920 | 0.9929             | 0.0009             |

Note: — = no calculation for this test number.

the theoretical ones quite well, with high MAC values. The mean of the five MAC values for the three scenarios are 0.99, 0.96, and 0.97, respectively. Scenario 2 gives the worst extracted mode shape, perhaps because only one transducer was fitted at midspan, which makes the bridge less homogenous than, for example, when five transducers are distributed evenly.

The identified mean damping ratios for the three scenarios are 0.0155, 0.0201, and 0.0270, respectively; whereas the corresponding theoretical values are 0.016, 0.021, and 0.043, respectively. The results for Scenarios 1 and 2 match the theoretical values very well, and the results for Scenario 3 show a greater error. This error is caused by the strong edge-effect result in the higher bridge damping ratio, which is consistent with the simulation studies. To overcome

this, the algorithm is slightly modified; that is, the MAC calculation does not consider the edge-effect section (in this study it simply ignores the last tenth of the entire bridge span). Therefore, the modal parameters are extracted again, and the results are listed in Table 5 (as Scenario 3\*). The mean damping ratio is identified as 0.0421, matching the theoretical one of 0.043 very well. Test no. 1 for Scenario 3\* is taken as an example and illustrated in Fig. 22. Apparently the higher damping ratio has a stronger edge effect compared with that of 1.6%. The noncorrected algorithm does not function at all for Scenario 3\*.

Note that both the extracted damping ratio and mode shape are very accurate for Scenario 1 compared with the theoretical values. When the bridge damping ratio is high, there is strong edge effect of

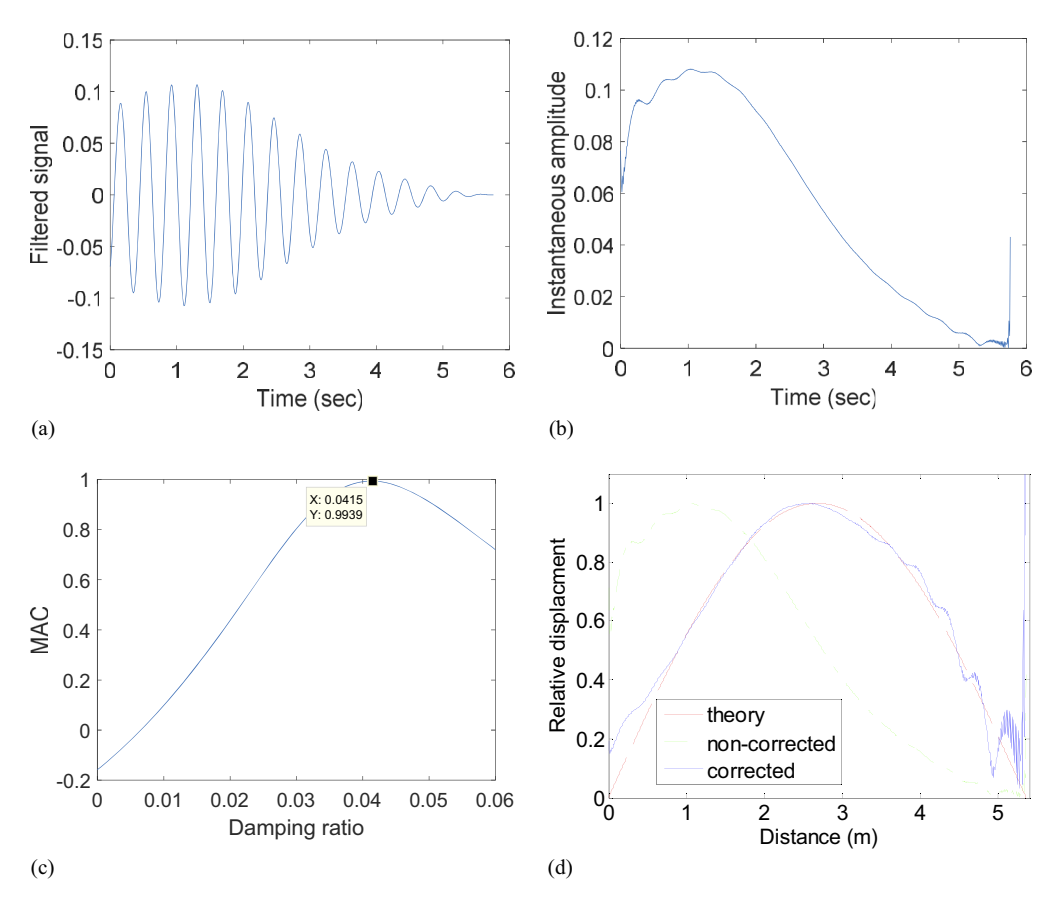


**Fig. 22.** Extraction of mode shape for Test no. 1, Scenario 3\*: (a) filtered signal; (b) corresponding instantaneous amplitude of HT; (c) damping ratio versus MAC; and (d) extracted mode shape.

the extracted mode shape, leading to a greater error in the damping ratio estimation. By ignoring this edge-effect section of MAC, one can obtain an accurate damping ratio, but the extracted mode shape is still contaminated at the edge-effect section. One promising approach to avoid this is to appropriately smooth the instantaneous amplitude of HT before reversing it as previously mentioned.

#### Conclusion

This study proposes an algorithm to extract bridge modal parameters, with a focus on damping ratio and mode shapes, using the dynamic response of a passing vehicle. The HT is applied to the filtered signals. The feasibility of the concept is established through theoretical analysis, numerical simulation, and laboratory experiments. It is demonstrated that the proposed algorithm greatly improves the extracted mode shape over the algorithm presented by Yang et al. (2014). A key limitation of the proposed algorithm at this time is a requirement for the vehicle to have a low and constant speed. Also, the high bridge damping generates a strong edge effect of the extracted mode shapes, negatively affecting the accuracy of the proposed algorithm. In the simulations, an increase in vehicle speed decreases the precision of the extracted results. The proposed algorithm also is shown to be capable of extracting the modal parameters of the second mode shape with relatively good precision. Although a band-pass filter can partially remove the random vibration caused by road roughness, even a road with a class A profile, i.e., in "very good" condition, has a negative impact on the proposed algorithm, especially for the higher modes.

The laboratory experiments provided further evidence of the potential of the proposed algorithm. The algorithm accurately identifies the bridge damping to detect the first increase by only using one sensor installed on the instrumented vehicle. In conclusion, the proposed algorithm is able to detect the change of bridge damping ratio and higher accuracy mode shapes, and it has the potential for application in the use of indirect measurement to monitor bridge health.

# Acknowledgments

The National Science of Foundation of the United States (grants NSF-CNS-1645863 and NSF-CSR-1813949) sponsored this research. Any opinions, findings, conclusions, or recommendations expressed in this publication are those of the authors and do not necessarily reflect the view of the sponsors.

#### References

Brady, S., E. Obrien, and A. Žnidarič. 2006. "Effect of vehicle velocity on the dynamic amplification of a vehicle crossing a simply supported bridge." *J. Bridge Eng.* 11 (2): 241–249. https://doi.org/10.1061/(ASCE)1084-0702(2006)11:2(241).

Carden, E. P., and P. Fanning. 2004. "Vibration based condition monitoring: A review." Struct. Health Monit. 3 (4): 355–377. https://doi.org/10.1177/1475921704047500.

Cebon, D. 1999. Handbook of vehicle-road interaction. Exton, PA: Swets & Zeitlinger.

- Chang, P. C., A. Flatau, and S. Liu. 2003. "Review paper: Health monitoring of civil infrastructure." Struct. Health Monit. 2 (3): 257–267. https://doi.org/10.1177/1475921703036169.
- Chrysostomou, C. Z., and A. Stassis. 2008. "Health-monitoring and systemidentification of an ancient aqueduct." Smart Struct. Syst. 4 (2): 183– 194. https://doi.org/10.12989/sss.2008.4.2.183.
- Deng, L., and C. Cai. 2009. "Identification of parameters of vehicles moving on bridges." *Eng. Struct.* 31 (10): 2474–2485. https://doi.org/10.1016/j.engstruct.2009.06.005.
- Deng, L., and C. Cai. 2010. "Bridge model updating using response surface method and genetic algorithm." J. Bridge Eng. 15 (5): 553–564. https:// doi.org/10.1061/(ASCE)BE.1943-5592.0000092.
- Deng, L., W. Yan, and L. Nie. 2019. "A simple corrosion fatigue design method for bridges considering the coupled corrosion-overloading effect." Eng. Struct. 178 (Jan): 309–317. https://doi.org/10.1016/j .engstruct.2018.10.028.
- Doebling, S. W., C. R. Farrar, and M. B. Prime. 1998. "A summary review of vibration-based damage identification methods." *Shock Vib. Dig.* 30 (2): 91–105. https://doi.org/10.1177/058310249803000201.
- Frýba, L. 2014. Vibration of solids and structures under moving loads. Dordrecht, Netherlands: Springer.
- González, A., E. J. Obrien, and P. J. McGetrick. 2012. "Identification of damping in a bridge using a moving instrumented vehicle." *J. Sound Vib.* 331 (18): 4115–4131. https://doi.org/10.1016/j.jsv.2012.04.019.
- Grande, E., and M. Imbimbo. 2016. "A multi-stage approach for damage detection in structural systems based on flexibility." *Mech. Syst. Signal Process.* 76–77 (Aug): 455–475. https://doi.org/10.1016/j.ymssp.2016.01.025.
- Hu, H., and J. Tang. 2005. "A convolution integral method for certain strongly nonlinear oscillators." J. Sound Vib. 285 (4–5): 1235–1241. https://doi.org/10.1016/j.jsv.2004.11.023.
- Huang, N. E. 2014. Hilbert–Huang transform and its applications. Singapore: Word Scientific.
- ISO. 1995. Mechanical vibration—Road surface profiles—Reporting of measured data. ISO 8608:1995. Geneva: ISO.
- Keenahan, J., E. J. Obrien, P. J. McGetrick, and A. Gonzalez. 2014. "The use of a dynamic truck-trailer drive-by system to monitor bridge damping." Struct. Health Monit. 13 (2): 143–157. https://doi.org/10.1177 /1475921713513974.
- Kim, C. W., R. Isemoto, P. J. McGetrick, M. Kawatani, and E. J. Obrien. 2014. "Drive-by bridge inspection from three different approaches." Smart Struct. Syst. 13 (5): 775–796. https://doi.org/10.12989/sss.2014 .13.5.775.
- Kim, C. W., R. Isemoto, T. Toshinami, M. Kawatani, P. McGetrick, and E. J. Obrien. 2011. "Experimental investigation of drive-by bridge inspection." In *Proc.*, 5th Int. Conf. on Structural Health Monitoring of Intelligent Infrastructure (SHMII-5). Mexico City, Mexico: Instituto de Ingenieria, UNAM.
- Kim, C. W., M. Kawatani, and K. B. Kim. 2005. "Three-dimensional dynamic analysis for bridge-vehicle interaction with roadway roughness." *Comput. Struct.* 83 (19–20): 1627–1645. https://doi.org/10.1016/j .compstruc.2004.12.004.
- Kong, X., C. Cai, and B. Kong. 2016. "Numerically extracting bridge modal properties from dynamic responses of moving vehicles." *J. Eng. Mech.* 142 (6): 04016025. https://doi.org/10.1061/(ASCE)EM.1943-7889.0001033.
- Kong, X., C. Cai, L. Deng, and W. Zhang. 2017. "Using dynamic responses of moving vehicles to extract bridge modal properties of a field bridge." *J. Bridge Eng.* 22 (6): 04017018. https://doi.org/10.1061/(ASCE)BE .1943-5592.0001038.
- Lin, C. W., and Y. B. Yang. 2005. "Use of a passing vehicle to scan the fundamental bridge frequencies: An experimental verification." Eng. Struct. 27 (13): 1865–1878. https://doi.org/10.1016/j.engstruct.2005.06.016.

- Magalhães, F., A. Cunha, and E. Caetano. 2012. "Vibration based structural health monitoring of an arch bridge: From automated OMA to damage detection." *Mech. Syst. Signal Process.* 28 (Apr): 212–228. https://doi. org/10.1016/j.ymssp.2011.06.011.
- Marulanda, J., J. M. Caicedo, and P. Thomson. 2017. "Mode shapes identification under harmonic excitation using mobile sensors." *Ing. Compet.* 19 (1): 165–173.
- Malekjafarian, A., and E. J. Obrien. 2014. "Identification of bridge mode shapes using Short Time Frequency Domain Decomposition of the responses measured in a passing vehicle." *Eng. Struct.* 81 (Dec): 386– 397. https://doi.org/10.1016/j.engstruct.2014.10.007.
- Malekjafarian, A., and E. J. Obrien. 2017. "On the use of a passing vehicle for the estimation of bridge mode shapes." *J. Sound Vib.* 397 (Jun): 77– 91. https://doi.org/10.1016/j.jsv.2017.02.051.
- McGetrick, P. J., A. González, and E. J. Obrien. 2009. "Theoretical investigation of the use of a moving vehicle to identify bridge dynamic parameters." *Insight* 51 (8): 433–438. https://doi.org/10.1784/insi.2009.51.8.433.
- McGetrick, P. J., C. W. Kim, A. González, and E. J. Obrien. 2015. "Experimental validation of a drive-by stiffness identification method for bridge monitoring." *Struct. Health Monit.* 14 (4): 317–331. https://doi.org/10.1177/1475921715578314.
- Obrien, E. J., and A. Malekjafarian. 2016. "A mode shape-based damage detection approach using laser measurement from a vehicle crossing a simply supported bridge." *Struct. Control Health Monit.* 23 (10): 1273–1286. https://doi.org/10.1002/stc.1841.
- Oshima, Y., K. Yamamoto, and K. Sugiura. 2014. "Damage assessment of a bridge based on mode shapes estimated by responses of passing vehicles." *Smart Struct. Syst.* 13 (5): 731–753. https://doi.org/10.12989/sss.2014.13.5.731.
- Tan, C., A. Elhattab, and N. Uddin. 2017. "Drive-by" bridge frequency-based monitoring utilizing wavelet transform." J. Civ. Struct. Health Monit. 7 (5): 615–625. https://doi.org/10.1007/s13349-017-0246-3.
- Tan, C., N. Uddin, and A. Elhattab. 2018. "Utilizing Hilbert Transform to assess the bridge health condition." In *Proc., ICVRAM ISUMA UNCERTAINTIES Conf.* Florianopolis, Brazil: ICVRAM ISUMA UNCERTAINTIES.
- Wang, W., L. Deng, and X. Shao. 2016. "Number of stress cycles for fatigue design of simply-supported steel I-girder bridges considering the dynamic effect of vehicle loading." Eng. Struct. 110 (Mar): 70–78. https://doi.org/10.1016/j.engstruct.2015.11.054.
- Yang, J. P., and W. C. Lee. 2018. "Damping effect of a passing vehicle for indirectly measuring bridge frequencies by EMD technique." *Int. J. Struct. Stab. Dyn.* 18 (1): 1850008. https://doi.org/10.1142 /S0219455418500086.
- Yang, Y. B., and K. C. Chang. 2009. "Extraction of bridge frequencies from the dynamic response of a passing vehicle enhanced by the EMD technique." J. Sound Vib. 322 (4–5): 718–739. https://doi.org/10.1016/j.jsv 2008 11 028
- Yang, Y. B., Y. C. Li, and K. C. Chang. 2014. "Constructing the mode shapes of a bridge from a passing vehicle: A theoretical study." *Smart Struct. Syst.* 13 (5): 797–819. https://doi.org/10.12989/sss.2014.13.5 .797.
- Yang, Y. B., and C. W. Lin. 2005. "Vehicle-bridge interaction dynamics and potential applications." *J. Sound Vib.* 284 (1–2): 205–226. https://doi.org/10.1016/j.jsv.2004.06.032.
- Yang, Y. B., C. W. Lin, and J. D. Yau. 2004a. "Extracting bridge frequencies from the dynamic response of a passing vehicle." *J. Sound Vib.* 272 (3–5): 471–493. https://doi.org/10.1016/S0022-460X(03)00378-X.
- Yang, Y. B., Z. Yao, and Y. Wu. 2004b. Vehicle-bridge interaction dynamics: With applications to high-speed railways. River Edge, NJ: World Scientific.
- Zhang, Y., L. Wang, and Z. Xiang. 2012. "Damage detection by mode shape squares extracted from a passing vehicle." *J. Sound Vib.* 331 (2): 291–307. https://doi.org/10.1016/j.jsv.2011.09.004.